Available online at BCREC website: https://bcrec.id

Bulletin of Chemical Reaction Engineering & Catalysis, 18 (4) 2023, 604-614

Research Article

Synthesis of ZnO/NiO/g-C_3N_4 Nanocomposite Materials for Photocatalytic Degradation of Tetracycline Antibiotic

Linh X. Nong[1,2], Oanh T. K. Nguyen[1,2,*]

[1]*Institute for Technology Application and Sustainable Development, Nguyen Tat Thanh University, Nguyen Tat Thanh, 700000, Viet Nam.*
[2]*Faculty of Environmental and Food Engineering, Nguyen Tat Thanh University, Ho Chi Minh City, 700000, Viet Nam.*

Received: 14th September 2023; Revised: 20th October 2023; Accepted: 20th October 2023
Available online: 23rd October 2023; Published regularly: December 2023

Abstract

In this study, an approach was utilized to improve the photocatalytic efficacy of g-C_3N_4 by creating a composite photocatalyst through co-precipitation. This process involved incorporating NiO and ZnO into the structure, resulting in enhanced photocatalytic activity. The Scanning Electron Microscopy (SEM) showcases interesting aggregation behavior, revealing extensive arrays of ZnO/NiO/g-C_3N_4 particles. Ultraviolet–Visible Diffuse Reflectance Spectroscopy (UV-Vis DRS) confirms the composite's strong light absorption, especially in the visible spectrum. X-ray diffraction (XRD) analysis provides conclusive evidence of successful material synthesis. The degradation of tetracycline antibiotics under visible light exposure demonstrates an impressive photochemical degradation efficiency of 78.43%. Additionally, the composite exhibits impressive cycles of reuse, retaining its high photocatalytic activity even after four reaction cycles. This performance surpasses that of comparison samples. The synergistic integration of NiO and g-C_3N_4 within ZnO proves to be crucial in enhancing photocatalytic activity by enhancing electron-hole separation and mitigating recombination processes. This composite photocatalyst shows a wide potential for efficiently eliminating tetracycline antibiotics from water systems.

Keywords: ZnO/NiO/g-C_3N_4; nanocomposites; tetracycline; co-precipitation

How to Cite: L.X. Nong, O.T.K. Nguyen (2023). Synthesis of ZnO/NiO/g-C_3N_4 Nanocomposite Materials for Photocatalytic Degradation of Tetracycline Antibiotic. *Bulletin of Chemical Reaction Engineering & Catalysis*, 18(4), 604-614 (doi: 10.9767/bcrec.20039)

Permalink/DOI: https://doi.org/10.9767/bcrec.20039

1. Introduction

Photocatalysis has emerged as a highly promising and versatile technology with a wide range of applications, including the degradation of toxic organic substances, bacterial inactivation, and wastewater treatment. This field encompasses catalytic reactions that are triggered by the absorption of light by a substrate, offering a sustainable and environmentally friendly approach to address pressing challenges in various industries [1–4].

Among the diverse semiconductor materials investigated as photocatalysts, titanium dioxide (TiO_2) has received significant attention due to its excellent chemical stability, low cost, non-toxicity, and strong oxidative capabilities. These properties have made TiO_2 a benchmark material in photocatalysis research. Under UV light irradiation, it has demonstrated remarkable efficiency in degrading organic pollutants into harmless byproducts, such as carbon dioxide and water. However, TiO_2 has limitations in

* Corresponding Author.
Email: ntkoanh.ntt.edu.vn (O.T.K. Nguyen);
Telp: +84-39-2073898

terms of its wide band gap, which restricts its absorption of visible light, thus hampering its photocatalytic activity under solar irradiation [5,6].

To overcome the limitations of TiO_2 and broaden the range of light absorption, researchers have explored alternative semiconductor photocatalysts [7]. One such material is graphitic carbon nitride (g-C_3N_4), which has garnered significant interest due to its unique electronic band structure, good light sensitivity, high physicochemical stability, and ability to capture visible light. The structure of g-C_3N_4 closely resembles graphene, consisting of a two-dimensional layered arrangement of carbon and nitrogen atoms [8]. Despite its advantages, g-C_3N_4 suffers from low surface area, rapid recombination of electron-hole pairs, poor conductivity, and limited absorption above 460 nm [9]. These drawbacks have prompted researchers to investigate strategies for enhancing the photocatalytic performance of g-C_3N_4, including modifying its morphological structure, introducing doping with metallic or non-metallic elements, and fabricating heterostructures [10–12].

In recent years, efforts have been focused on developing composite photocatalysts that combine multiple semiconductor materials to harness their synergistic effects and improve overall performance. One such composite is the ZnO/NiO/g-C_3N_4 system, which offers unique advantages derived from each constituent material. Zinc oxide (ZnO), a low-cost and highly chemically stable semiconductor, has been extensively studied and widely employed in electronics, materials, and energy applications [13,14]. However, its photocatalytic performance is limited by its relatively high band gap energy, resulting in inadequate absorption of visible light and diminished photocatalytic efficiency. Researchers have explored various strategies, such as metal or non-metal ion doping and surface modification, to enhance ZnO light absorption and extend its photocatalytic activity into the visible light region to address this [15,16].

Nickel oxide (NiO), another promising semiconductor, has gained attention as a photocatalyst for environmental remediation, particularly in aquatic environments. NiO can efficiently decompose pollutants, including organic compounds, anions, cations, and toxic substances, under sunlight or UV light irradiation. Moreover, NiO exhibits non-toxic and environmentally friendly properties [17]. However, challenges related to reproducibility and particle size control have prompted further research to enhance NiO's catalytic efficiency and stability. Various strategies, such as combining NiO with carbon nanotubes (CNTs) or doping it with transition metals, have been explored to improve its photocatalytic performance [18].

This research aims to synthesize the ZnO/NiO/g-C_3N_4 composite through a co-precipitation technique and analyze its effectiveness in photocatalytically degrading tetracycline, a prevalent antibiotic pollutant found in wastewater. Tetracycline is known to persist in the environment and can harm ecosystems. The composite will be subjected to LED light sources to evaluate its performance when exposed to visible light. The study will investigate the photocatalytic degradation efficiency and the potential for reuse of the composite as a photocatalyst for removing organic pollutants.

2. Materials and Methods

2.1 Materials

In this study, the following chemicals were utilized: Urea ($(NH_2)_2CO$, 99%, Xilong Chemical, China), Nickel(II) nitrate hexahydrate ($Ni(NO_3)_2.6H_2O$, 96%, Guangdong Chemical, China), Zinc nitrate hexahydrate ($Zn(NO_3)_2.6H_2O$, 99.5%, Damao Chemical, China), sodium hydroxide (NaOH, 96%, Xilong Chemical, China), Tetracycline (TCC, 95%, Sigma-Aldrich, European), tert-Butanol (TBA, 99.5%, Sigma-Aldrich, USA), p-Benzoquinone (BQ, 98%, Sigma-Aldrich, USA), Potassium dichromate ($K_2Cr_2O_7$, 99.8%, Xilong Chemical, China), Sodium oxalate ($Na_2C_2O_4$, 99.8%, Xilong Chemical, China). All materials are of analytical grade and utilized without further purification before the synthesis process.

2.2 Synthesis of Catalysts

In this study, g-C_3N_4 was synthesized by thermal decomposition of urea according to the following specific process: First, 10 g of urea was put into a porcelain crucible. Next, the material was placed in a porcelain crucible, which was heated to 550 °C at a heating rate of 10 °C/min in a furnace and for 3 h in air. Finally, the porcelain crucible is cooled down to room temperature after the reaction. The obtained g-C_3N_4 (CN) material was used for further experiments.

ZnO/NiO/g-C_3N_4 (ZNG) composites were synthesized by the co-precipitation method. First, 5.94 g of $Zn(NO_3)_2.6H_2O$ and 5.81 g of $Ni(NO_3)_2.6H_2O$ were dissolved in 100 mL of distilled water. Then, g-C_3N_4 with 200 mg was dispersed in the beaker, and 100 mL of NaOH

solution (2 M) was added to the mixture and stirred for 2 h. The final product was washed with distilled water and ethanol and dried for 12 h. Finally, the material was calcined at 550 °C (2 °C/min) for 2 h. After calcination, the powder was finely ground for further analysis. In addition, ZnO/NiO (ZN), ZnO/g-C_3N_4 (ZG), and NiO/g-C_3N_4 (NG) materials were synthesized using the same method.

2.3 Instruments

The crystalline structures of the prepared samples were examined by X-ray diffraction (XRD, D8 Advance, Bruker, USA). We used a Cary 4000 UV-visible spectrophotometer from Agilent (USA) to obtain the UV-visible diffuse reflectance spectra of the as-prepared sample. The existence of chemical bonds and functional groups was analyzed using a Fourier transform-infrared (FT-IR) spectrometer (EQUINOX 55, Bruker, USA). The microstructures of the as-prepared samples were evaluated using scanning electron microscopy (SEM, JSM 7401F, JEOL, USA). AUTOLAB-PGSTAT204 electrochemical analyzer was used to conduct electrochemical tests.

2.4 Photocatalytic Activity Test

To evaluate the photocatalytic activity of the as-prepared samples in the presence of TCC antibiotics, the following steps were followed under visible light irradiation using a white LED lamp with a power output of 40 W. The catalyzed samples were combined with TC antibiotics at a concentration of 20 ppm, with a catalyst concentration of 0.05 g/L. The reaction solution was stirred in the dark for 30 min, and samples were collected over 15 min. Subsequently, the samples were exposed to the white LED lamp, and at specific time intervals (*e.g.*, 45 min, 90 min, 135 min, *etc.*), samples were taken out. After extraction, the samples were centrifuged at 7000 rpm for 10 min to ensure complete removal of any solid particles. The results were measured using a UV-Vis instrument. To validate the cycling performance of the catalyst we prepared, following the initial photocatalytic test, the catalyst was subjected to filtration and rinsing employing ethanol and water. Subsequently, the catalyst was dried and employed for a subsequent run. This recycling process was iterated for a total of four cycles.

Additionally, to identify and scavenge the free radicals responsible for the degradation of TCC, electron capture experiments were conducted under the same experimental conditions as the photodegradation study. These additional experiments aimed to pinpoint and neutralize the specific free radicals by introducing electron-capturing agents, also known as scavengers, into the solution before exposure to light. The substances used for this purpose included TBA (•OH), BQ ($\bullet O_2^-$), $K_2Cr_2O_7$ (e^-), and $Na_2C_2O_4$ (h^+).

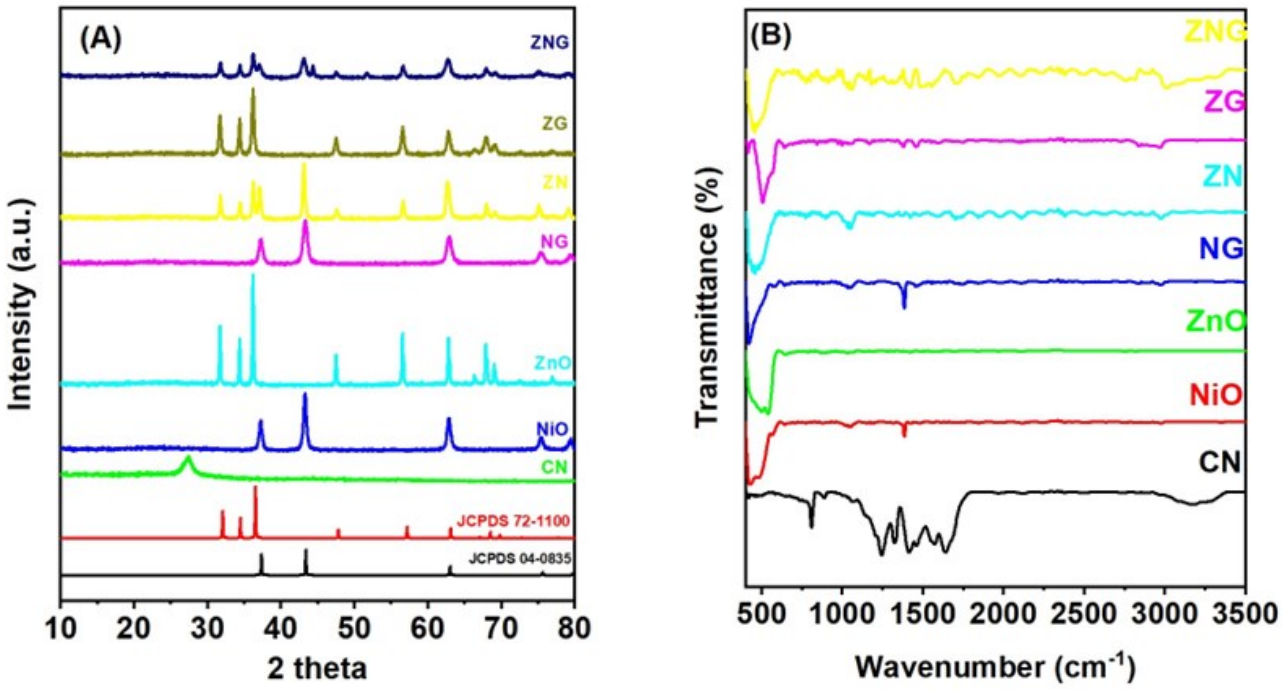

Figure 1. (A) XRD pattern of the as-prepared sample, (B) FT-IR spectra of the synthesized samples.

3. Results and Discussion

3.1 Crystal Structure and Morphological Characteristics

Figure 1(A) presents the XRD results for several samples, including CN, ZnO, NiO, ZG, NG, ZN, and ZNG. The diffraction patterns obtained for all synthesized samples aligned with the standard positions corresponding with wurtzite ZnO (JCPDS file 72-1100) and NiO (JCPDS 04-0835). Importantly, slight changes in the lower angle (2θ) values and broader main peaks at 31.75°, 34.38°, and 36.14° are observed in the XRD patterns of the ZN and ZNG samples. These observations confirm the successful incorporation of NiO into ZnO and the integration of NiO/ZnO with g-C_3N_4. Notably, the doping of NiO into ZnO does not alter the overall structure or introduce any new diffraction peaks in the XRD patterns of the ZN and ZNG samples. The XRD pattern of pure CN exhibits a prominent peak at 27.4°, indicating the presence of nanolayers in g-C_3N_4, consistent with previous research findings [19–21]. However, in the XRD pattern of the ZNG composite, the diffraction peaks of the g-C_3N_4 sample are not observed due to the higher content of NiO and ZnO [22,23].

The FTIR spectra in Figure 1(B) showed the samples CN, ZnO, NiO, ZG, NG, ZN, and ZNG. The appearance of an additional peak at 550 cm^{-1} is attributed to the presence of NiO as an impurity incorporated into the structure of NiO/ZnO nanoparticles, resulting in a sharper peak. The peaks at 420 cm^{-1} and 430 cm^{-1} are assigned to the combined absorption of ZnO and NiO bonds. Furthermore, the substitution of NiO for ZnO positions has been detected in the spectra peaks at 670 cm^{-1} [24]. Spectral peaks related to water absorption on NiO/ZnO catalysts appear around 1700 cm^{-1}. The peak at 1645 cm^{-1} is explained by the stretching vibration mode of the C–N group, and the peaks at 1570 cm^{-1}, 1408 cm^{-1}, 1319 cm^{-1}, and 1238 cm^{-1} may be attributed to the stretching vibrations of aromatic C–N bonds. The peak at 812

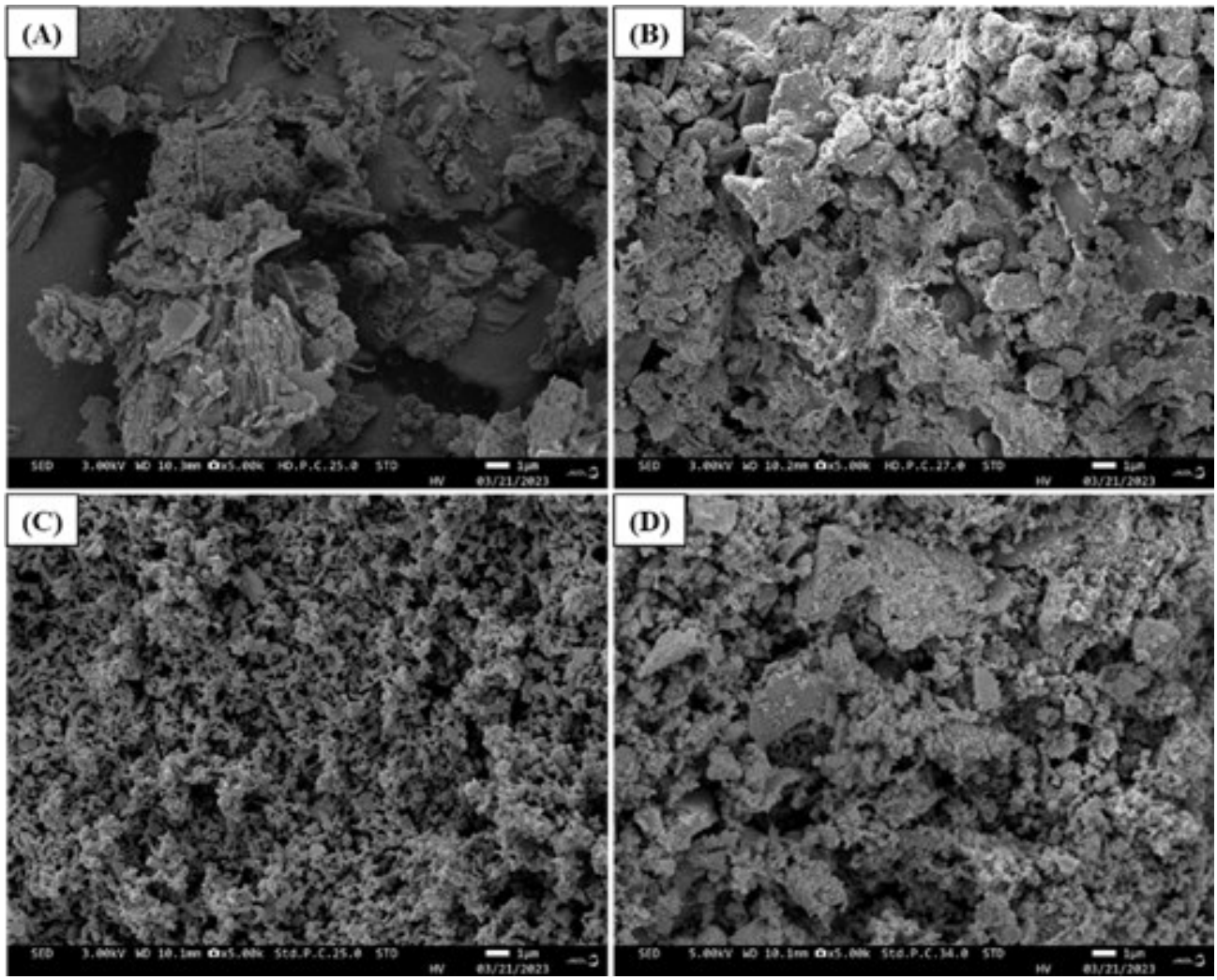

Figure 2. SEM images of samples: (A) CN, (B) NiO, (C) ZnO, and (D) ZNG.

cm^{-1} corresponds to the stretching vibration mode of the triazine structure. The peak at 3161 cm^{-1} indicates the stretching vibration mode of the N–H group [25].

The SEM images of the prepared samples (Figure 2) show that pure NiO has a nanoparticle morphology. ZnO also exhibits a similar nanoparticle morphology, while CN has a stacked plate structure. After doping NiO and ZnO, the ZNG mixture tends to aggregate into large arrays, regardless of the shape of CN. This aggregation, as shown in Figure 2, enhances the specific surface area and improves the material's ability to degrade antibiotics effectively.

In Figure 3(a) and Table 1, the bandgap energies of the synthesized samples were estimated. The UV-visible spectra of the prepared sample were determined using the Tauc plot equation (Equation (1)).

$$(\alpha hv) = A(hv - Eg)^n \quad (1)$$

Here, α is the absorption coefficient, A is a constant, and n = 1/2 for a direct band gap material. The majority of the synthesized samples exhibit a narrow absorbance in the ultraviolet (UV) light region. However, ZNG demonstrates enhanced light absorption and a shift in the absorption edge towards the visible light range compared to the other samples. This increased light absorption and shift towards visible light in ZNG were consistent with previous studies on synthesized materials that had been specifically designed to possess visible light absorption properties.

Furthermore, the enhancement of electron-hole separation by ZNG was demonstrated through electrochemical impedance spectroscopy (EIS) analysis. Figure 3(b) illustrates the EIS spectra of the prepared samples. Compared to the other samples, ZNG exhibits a smaller arc radius in the EIS Nyquist plot, indicating more efficient transfer and separation of photogenerated charge carriers on the perovskite structure. This observation highlights the effective separation of photoinduced electron-hole pairs in ZNG.

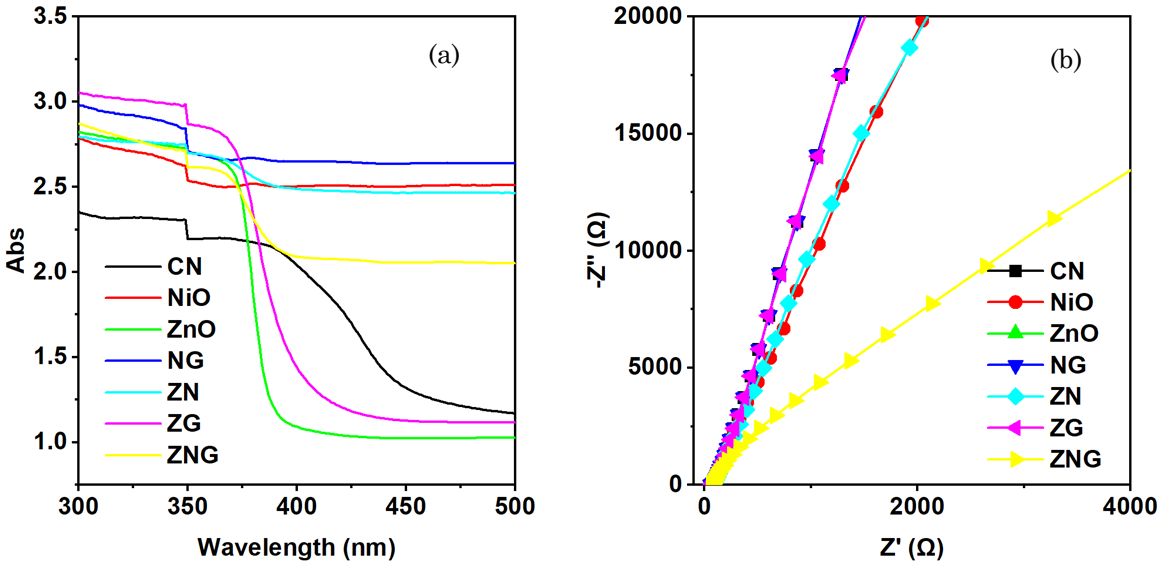

Figure 3. (a) UV-Vis DRS and (b) EIS spectra of the synthesized samples.

Table 1. Band gap energy and kinetic parameters of photocatalytic reactions by different samples.

Sample	*Eg* (eV)	*k* (min^{-1})	R^2
CN	2.64	0.0013	0.97482
NiO	3.20	0.0004	0.95326
ZnO	3.05	0.0025	0.94112
NG	2.90	0.0004	0.80211
ZG	2.96	0.0021	0.9609
ZN	2.97	0.0016	0.8905
ZNG	2.62	0.0065	0.9747

3.2 Photocatalytic Performance

In Figure 4, the photocatalytic activity of the synthesized samples against 20 ppm TCC antibiotic was shown. The results reveal that the ZNG sample exhibited the highest decomposition activity of 78.43% after 300 min of light exposure, surpassing the activity of the other samples. Furthermore, the UV-Vis analysis of the sample shows no significant shift in the absorption peak of TCC (357 nm), and the photodegradation of TCC in the absence of the material is negligible. This result confirms that the ZNG sample has good photocatalytic activity, as the combination of CN, ZnO, and NiO assisted in decomposing antibiotics under visible light.

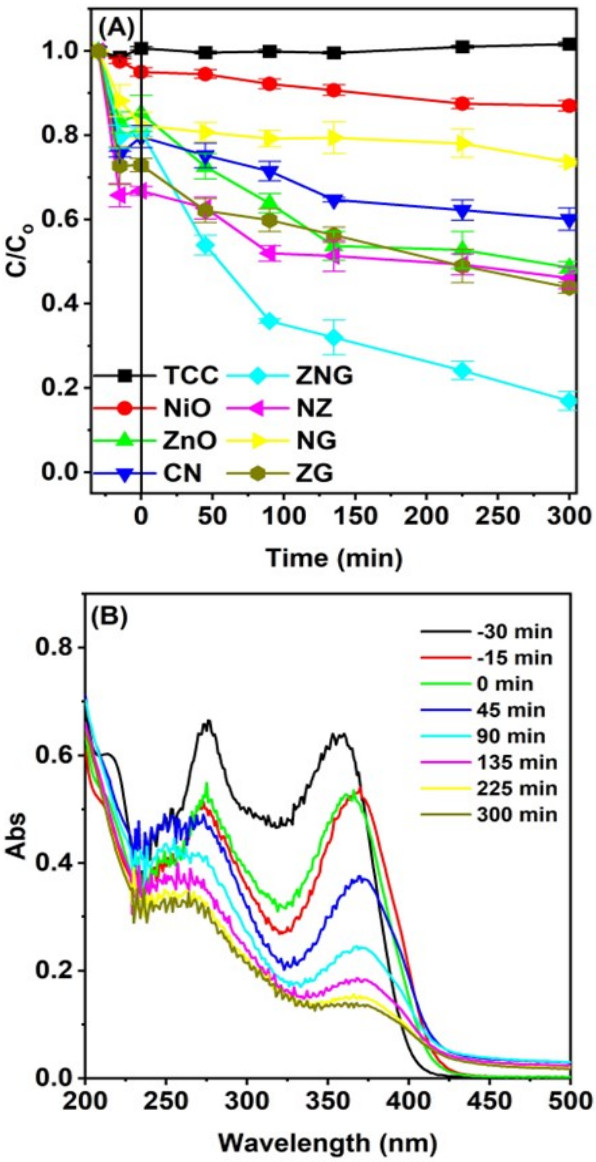

Figure 4. (A) Photocatalytic degradation of as-prepared samples under visible light. (B) The UV-vis absorption spectra were obtained for the photodegradation reaction of the ZNG sample.

Figure 5 indicated that the presence of $Na_2C_2O_4$, $K_2Cr_2O_7$, TBA, BQ, and the initial sample had a varied impact on the degradation yield and overall efficiency of the optimal photocatalyst. $Na_2C_2O_4$ shows a significant reduction in degradation yield (9.18%), suggesting its inhibitory effect on the photocatalytic process. Similarly, $K_2Cr_2O_7$, TBA, and BQ also contribute to reduced degradation yields of 68.32%, 73.29%, and 15.77%, respectively, indicating their interference with the photocatalytic efficiency. Furthermore, the initial sample has the highest degradation efficiency of up to 78.43%. These results suggest that the electron capturers partially hinder the photocatalytic performance, while $Na_2C_2O_4$ specifically impedes the TCC antibiotic degradation, high-

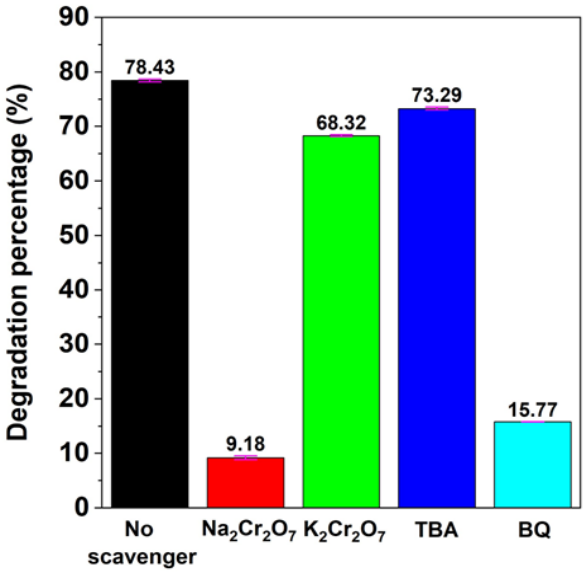

Figure 5. Effect of electron captures on the degradation of TCC.

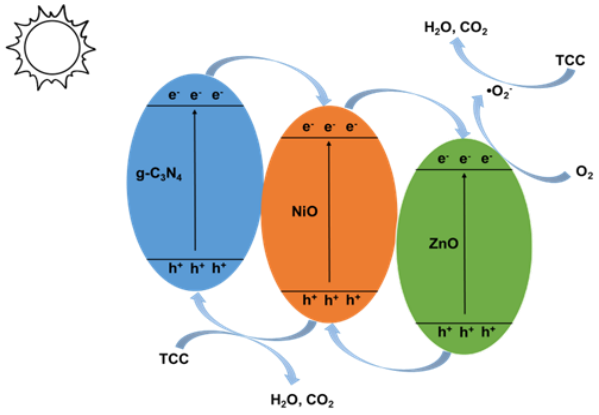

Figure 6. Photocatalytic mechanism diagram of ZNG sample.

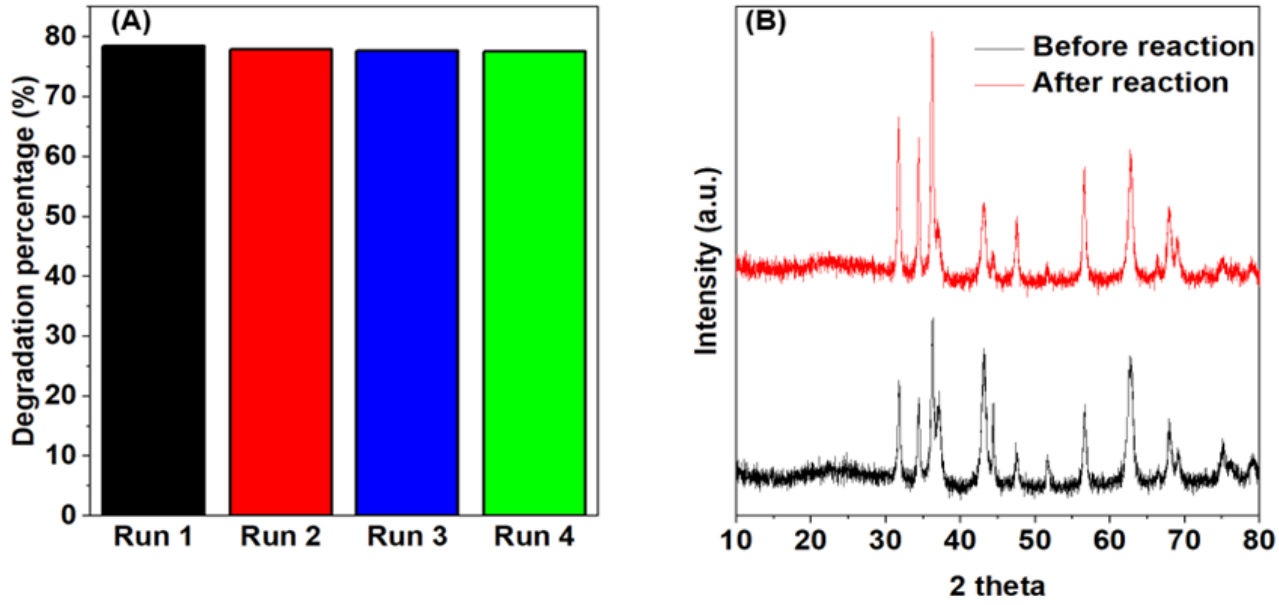

Figure 7. (A) Experiment to evaluate the durability of the material, (B) XRD spectrum of the material before and after the reaction.

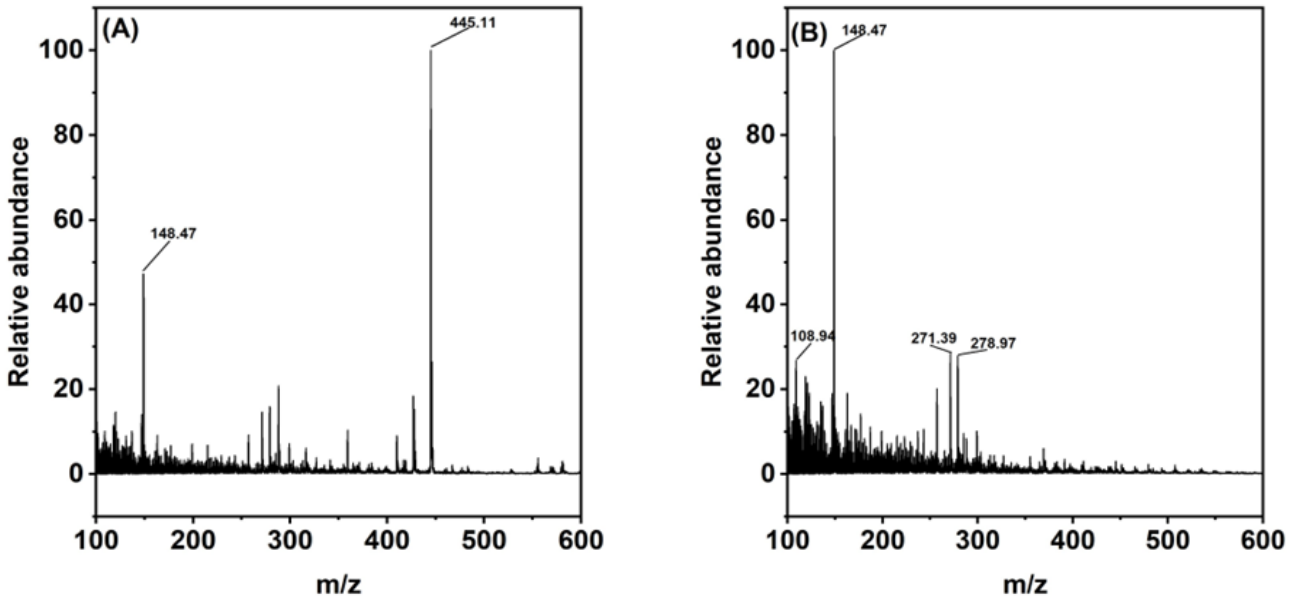

Figure 8. The main by-products of TCC degradation were detected by LC-MS.

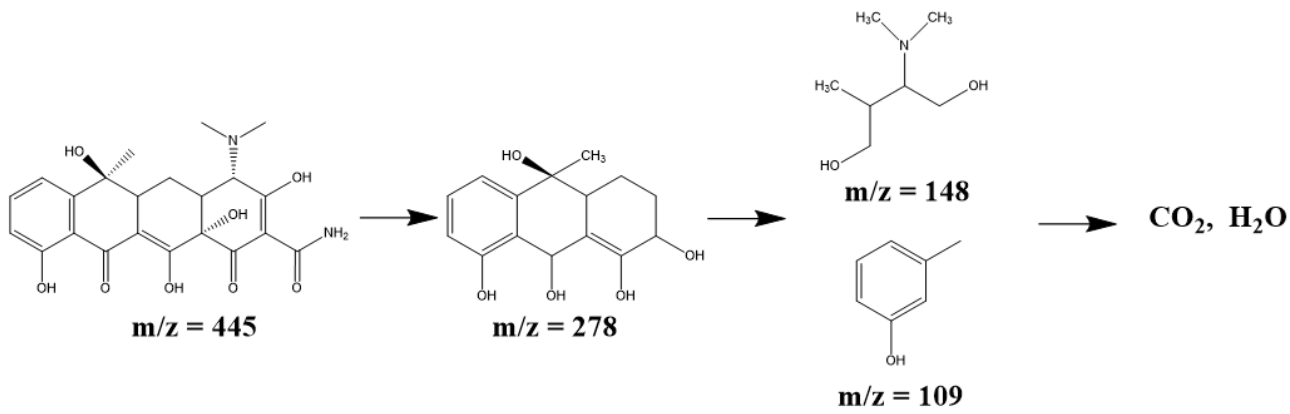

Figure 9. Proposed degradation pathways of TCC.

Table 2. Compare the degradation efficiency of various photocatalysts.

Photocatalyst	Reaction parameters	Band gap energy (eV)	Light source	Organic compound	Degradation efficiency	Ref.
ZnO/NiO/g-C_3N_4	co-precipitation	2.62	40 W white LED	Tetracycline	78.43% Tetracycline after 300 min	This word
g-C_3N_4/Ni-ZnO	co-precipitation	2.25	Under sunlight	Methylene blue	89.45 % Methylene blue after 90 min	[33]
g-C_3N_4/Mn-doped ZnO	co-precipitation	-	Under sunlight	Methylene blue	Methylene blue (100%) after 60 min	[34]
Cu doped ZnO/g-C_3N_4	one-pot pyrolysis	3.0	500 W Xe light	Eriochrome Black T	99% after 90 min	[35]
g-C_3N_4/NiO/ZnO/Fe_3O_4	hydrothermal	2.8	Philips 23 W white LED	Esomeprazole	95.05% within 70 min	[36]
CuO/ZnO/g-C_3N_4	solution combustion	-	400 W hallow lamp	Methylene blue	98% within 45 min	[37]
ZnO/Au/g-C_3N_4	liquid phase pulsed laser	3.09	300 W Xe lamp	Methylene blue	99% within 120 min	[38]
g-C_3N_4/Ce-ZnO/Ti	electrophoretic deposition	-	36-72 W LED	Cefixime	80 % within 180 min	[39]
ZnO/g-C_3N_4	Physic mixing calcination	3.195	Hg lamp 250 W	methylene blue	93.2 % within 90 min	[40]

lighting the crucial role of h^+ in the photocatalytic mechanism.

CN functions as a photon absorber within the visible radiation spectrum, facilitating the excitation of electrons from the valence band to its conduction band (Figure 6). This process creates a vacancy, or hole (h^+), in the valence band. Notably, recent investigations have demonstrated that the conduction band potential of CN surpasses that of NiO and, by extension, exceeds that of ZnO [26,27]. This distinctive property prompts the migration of photoexcited electrons (e^-) from the conduction band of g-C_3N_4 to that of NiO, subsequently facilitating their transition to the conduction band of ZnO. Conversely, h^+ travel in the opposing direction: from the valence band of ZnO to the valence band of NiO, ultimately finding their destination within the valence band of g-C_3N_4. In parallel, the interaction between electrons within the conduction band of ZnO and adsorbed oxygen molecules (O_2) engenders the creation of anionic superoxide radicals ($\cdot O_2^-$). It is pertinent to note that the valence band energy of g-C_3N_4 is insufficient to catalyze the formation of hydroxyl radicals ($\cdot$OH), precluding the oxidation of H_2O into $\cdot$OH [28]. Upon their emergence, these radicals work together to attack TCC compounds, causing the antibiotic to break down.

The stability of the catalysts is an essential parameter that needs to be demonstrated for the practical applicability of the material. To confirm its stability, the reusability of the ZNG sample was tested through four cycles of TCC decomposition under the same conditions. The results reveal that a gradual decrease in TCC degradation efficiency after each cycle (Figure 7). This decrease could be attributed to either the loss of catalyst in each cycle or the coverage of some active sites on the surface of ZNG by TCC. Despite this decrease, the recycled material maintains a relatively good photocatalytic activity even after being reused four times. The degradation performance of the material after being reused four times is measured at 78.43%, 77.93%, 77.66%, and 73.52%, respectively, within 300 minutes. Following the fourth cycle, XRD analysis was conducted to assess the material's structural integrity. The results indicate that there are no significant changes observed in the material after the TCC antibiotic removal reaction. Furthermore, ZNG shows promising photocatalytic activity when compared to recent studies on composite photocatalysts, as reported in Table 2. This observation demonstrates the ZNG sample's ability to decompose toxic substances and suggests that its

stability was relatively good. The LC-MS spectrum accommodated valuable insights into the potential pathway of intermediate compound formation during the degradation of TCC observed in Figures 8 and 9. This analytical technique provides valuable insights into the transformations occurring during the degradation process of TCC, elucidating its mechanistic pathway and associated degradation products. The peak corresponding to TCC (m/z = 455) has notably decreased due to the photo-induced degradation of TCC during the photocatalytic process. Additionally, several new peaks have emerged after 300 minutes of degradation, corresponding to the degradation intermediates (m/z = 109, 148, 271, 278) [29–32].

4. Conclusions

ZNG nanocomposites were successfully synthesized using the co-precipitation method. The resulting nanocomposites exhibit large arrays as the ZnO, NiO, and CN components clumped together. Notably, the nanocomposites display an absorption edge that extends toward the visible light range, indicating their potential for visible light photocatalysis. Regarding photocatalytic activity, the nanocomposites achieve a TCC photodegradation efficiency of 78.43%. Furthermore, the stability of the nanocomposites is assessed after four reaction cycles, and they exhibit good performance, indicating their durability and potential for repeated use. In conclusion, the synthesized ZNG nanocomposites demonstrate promising photocatalytic properties, with high TCC photodegradation efficiency, absorption in the visible light range, and good stability over multiple reaction cycles.

Acknowledgment

This study was supported by NTTU Foundation for Science and Technology Development.

CRediT Author Statement

Author Contributions: Linh X. Nong: Conceptualization, Methodology, Investigation, Resources, Data Curation, Writing; Oanh T. K. Nguyen: Review and Editing, Supervision.

References

[1] Ghasemi, A. (2022). Nanoferrite photocatalysts. In A. Ghasemi *Magnetic Ferrites and Related Nanocomposites*, Elsevier. p. 521–585. DOI: 10.1016/B978-0-12-824014-4.00006-8.

[2] Sakka, S. (2013). Sol–Gel Process and Applications. In S. Somiya *Handbook of Advanced Ceramics*, Elsevier. p. 883–910. DOI: 10.1016/B978-0-12-385469-8.00048-4.

[3] Wang, D., Yin, F.X., Cheng, B., Xia, Y., Yu, J.G., Ho, W.K. (2021). Enhanced photocatalytic activity and mechanism of CeO_2 hollow spheres for tetracycline degradation. *Rare Metals*, 40, 2369–2380. DOI: 10.1007/S12598-021-01731-2.

[4] Xu, C., Zhou, Q., Huang, W.Y., Yang, K., Zhang, Y.C., Liang, T.X., Liu, Z.Q. (2022). Constructing Z-scheme ß-Bi_2O_3/ZrO_2 heterojunctions with 3D mesoporous SiO_2 nanospheres for efficient antibiotic remediation via synergistic adsorption and photocatalysis. *Rare Metals*, 41, 2094–2107. DOI: 10.1007/S12598-021-01897-9.

[5] Subramaniam, M.N., Goh, P.S., Lau, W.J., Ng, B.C., Ismail, A.F. (2019). Development of nanomaterial-based photocatalytic membrane for organic pollutants removal. In W.J. Lau, A.F. Ismail, A. Isloor, A. Al-Ahmed *Advanced Nanomaterials for Membrane Synthesis and Its Applications*, Elsevier. p. 45–67. DOI: 10.1016/B978-0-12-814503-6.00003-3.

[6] Sushma, S., Yadav, A. (2020). Biological and physicochemical combination processes. In A. Abdeltif, A.A. Assadi, P. Nguyen-Tri, T.A. Nguyen, S. Rtimi *Nanomaterials for Air Remediation*, Elsevier. p. 361–372. DOI: 10.1016/B978-0-12-818821-7.00018-X.

[7] Shu, T., Yang, W., Li, K., Yan, L., Dai, Y., Guo, H. (2015). Design of Silver-Deposited Carbon Nitride Nanotubes by a One-Step Solvothermal Treatment Strategy and Their Efficient Visible-Light Photocatalytic Activity Toward Methyl Orange Degradation. *Energy and Environment Focus*, 4, 107–115. DOI: 10.1166/eef.2015.1143.

[8] Liu, G., Huang, Y., Lv, H., Wang, H., Zeng, Y., Yuan, M., Meng, Q., Wang, C. (2021). Confining single-atom Pd on g-C_3N_4 with carbon vacancies towards enhanced photocatalytic NO conversion. *Applied Catalysis B: Environmental*, 284, 119683. DOI: 10.1016/j.apcatb.2020.119683.

[9] Fu, Y., Huang, T., Zhang, L., Zhu, J., Wang, X. (2015). Ag/g-C_3N_4 catalyst with superior catalytic performance for the degradation of dyes: a borohydride-generated superoxide radical approach. *Nanoscale*, 7, 13723–13733. DOI: 10.1039/C5NR03260A.

[10] Lin, P., Shen, J., Tang, H., Zulfiqar, Lin, Z., Jiang, Y. (2019). Enhanced photocatalytic H2 evolution of ultrathin g-C_3N_4 nanosheets via surface shuttle redox. *Journal of Alloys and Compounds*, 810, 151918. DOI: 10.1016/j.jallcom.2019.151918.

[11] Wang, Y., Zhao, X., Cao, D., Wang, Y., Zhu, Y. (2017). Peroxymonosulfate enhanced visible light photocatalytic degradation bisphenol A by single-atom dispersed Ag mesoporous g-C_3N_4 hybrid. *Applied Catalysis B: Environmental*, 211, 79–88. DOI: 10.1016/j.apcatb.2017.03.079.

[12] Wang, F., Wang, Y., Feng, Y., Zeng, Y., Xie, Z., Zhang, Q., Su, Y., Chen, P., Liu, Y., Yao, K., Lv, W., Liu, G. (2018). Novel ternary photocatalyst of single atom-dispersed silver and carbon quantum dots co-loaded with ultrathin g-C_3N_4 for broad spectrum photocatalytic degradation of naproxen. *Applied Catalysis B: Environmental*, 221, 510–520. DOI: 10.1016/j.apcatb.2017.09.055.

[13] Modares, M., Alijani, S., Nasernejad, B. (2022). NOx photocatalytic degradation over ZnO–CdS heterostructure composite under visible light irradiation. *Research on Chemical Intermediates*, 48, 1831–1845. DOI: 10.1007/s11164-022-04705-w

[14] Vu, A.-T., Mac, V.H., Nguyen, T.H., Nguyen, T.H. (2023). Preparation of carnation-like Ag-ZnO composites for enhanced photocatalysis under visible light. *Nanotechnology*, 34, 275602. DOI: 10.1088/1361-6528/acca24.

[15] Kumala, W. (2020). Synthesis and photocatalytic activity studies of Silver-Nitrogen co-doped ZnO-Fe_2O_3 nanocomposites for the degradation of Methylene blue under UV-Visible region. *Mediterranean Journal of Chemistry*, 10, 659. DOI: 10.13171/mjc107020071461wk.

[16] Bian, H., Zhang, Z., Xu, X., Gao, Y., Wang, T. (2020). Photocatalytic activity of Ag/ZnO /AgO/TiO_2 composite. *Physica E: Low-Dimensional Systems and Nanostructures*, 124, 114236. DOI: 10.1016/j.physe.2020.114236.

[17] Alkallas, F.H., Toghan, A., Ahmed, H.A., Alrefaee, S.H., Pashameah, R.A., Alrebdi, T.A., Mwafy, E.A., Mostafa, A.M. (2022). Catalytic performance of NiO nanoparticles decorated carbon nanotubes via one-pot laser ablation method against methyl orange dye. *Journal of Materials Research and Technology*, 18, 3336–3346. DOI: 10.1016/j.jmrt.2022.04.010.

[18] Far, H., Hamici, M., Brihi, N., Haddadi, K., Boudissa, M., Chihi, T., Fatmi, M. (2022). High-performance photocatalytic degradation of NiO nanoparticles embedded on α-Fe_2O_3 nanoporous layers under visible light irradiation. *Journal of Materials Research and Technology*, 19, 1944–1960. DOI: 10.1016/j.jmrt.2022.05.159.

[19] Pal, B., Sarkar, D., Giri, P.K. (2015). Structural, optical, and magnetic properties of Ni doped ZnO nanoparticles: Correlation of magnetic moment with defect density. *Applied Surface Science*, 356, 804–811. DOI: 10.1016/j.apsusc.2015.08.163.

[20] Lin, L.-S., Cong, Z.-X., Li, J., Ke, K.-M., Guo, S.-S., Yang, H.-H., Chen, G.-N. (2014). Graphitic-phase C_3N_4 nanosheets as efficient photosensitizers and pH-responsive drug nanocarriers for cancer imaging and therapy. *Journal of Materials Chemistry B*, 2, 1031. DOI: 10.1039/c3tb21479f.

[21] Di, G., Zhu, Z., Zhang, H., Zhu, J., Qiu, Y., Yin, D., Küppers, S. (2019). Visible-light degradation of sulfonamides by Z-scheme ZnO/g-C_3N_4 heterojunctions with amorphous Fe_2O_3 as electron mediator. *Journal of Colloid and Interface Science*, 538, 256–266. DOI: 10.1016/j.jcis.2018.11.100.

[22] Alman, V., Singh, K., Bhat, T., Sheikh, A., Gokhale, S. (2020). Sunlight Assisted improved photocatalytic degradation of rhodamine B using Pd-loaded g-C_3N_4/WO_3 nanocomposite. *Applied Physics A: Materials Science and Processing*, 126, 724. DOI: 10.1007/S00339-020-03914-7.

[23] Cao, J., Qin, C., Wang, Y., Zhang, H., Sun, G., Zhang, Z. (2017). Solid-state method synthesis of SnO2-decorated g-C_3N_4 nanocomposites with enhanced gas-sensing property to ethanol. *Materials*, 10(6), 604. DOI: 10.3390/ma10060604.

[24] Raja, K., Ramesh, P.S., Geetha, D. (2014). Synthesis, structural and optical properties of ZnO and Ni-doped ZnO hexagonal nanorods by Co-precipitation method. *Spectrochimica Acta Part A: Molecular and Biomolecular Spectroscopy*, 120, 19–24. DOI: 10.1016/j.saa.2013.09.103.

[25] Qi, K., Li, Y., Xie, Y., Liu, S., Zheng, K., Chen, Z., Wang, R. (2019). Ag Loading Enhanced Photocatalytic Activity of g-C_3N_4 Porous Nanosheets for Decomposition of Organic Pollutants. *Frontiers in Chemistry*, 7, 91. DOI: 10.3389/fchem.2019.00091.

[26] Derikvandi, H., Nezamzadeh-Ejhieh, A. (2017). Increased photocatalytic activity of NiO and ZnO in photodegradation of a model drug aqueous solution: Effect of coupling, supporting, particles size and calcination temperature. *Journal of Hazardous Materials*, 321, 629–638. DOI: 10.1016/j.jhazmat.2016.09.056.

[27] Goto, Y., Hisatomi, T., Wang, Q., Higashi, T., Ishikiriyama, K., Maeda, T., Sakata, Y., Okunaka, S., Tokudome, H., Katayama, M., Akiyama, S., Nishiyama, H., Inoue, Y., Takewaki, T., Setoyama, T. Minegishi, T., Takata, T., Yamada, T., Domen, K. (2018). A Particulate Photocatalyst Water-Splitting Panel for Large-Scale Solar Hydrogen Generation. *Joule*, 2(3), 509–520. DOI: 10.1016/j.joule.2017.12.009.

[28] He, Y., Cai, J., Li, T., Wu, Y., Lin, H., Zhao, L., Luo, M. (2013). Efficient degradation of RhB over $GdVO_4$/g-C_3N_4 composites under visible-light irradiation. *Chemical Engineering Journal*, 215–216, 721–730. DOI: 10.1016/J.CEJ.2012.11.074.

[29] Nie, M., Li, Y., He, J., Xie, C., Wu, Z., Sun, B., Zhang, K., Kong, L., Liu, J. (2020). Degradation of tetracycline in water using Fe_3O_4 nanospheres as Fenton-like catalysts: kinetics, mechanisms and pathways. *New Journal of Chemistry*, 44, 2847–2857. DOI: 10.1039/D0NJ00125B.

[30] Shi, W., Shu, K., Sun, H., Ren, H., Li, M., Chen, F., Guo, F. (2020). Dual enhancement of capturing photogenerated electrons by loading CoP nanoparticles on N-deficient graphitic carbon nitride for efficient photocatalytic degradation of tetracycline under visible light. *Separation and Purification Technology*, 246, 116930. DOI: 10.1016/j.seppur.2020.116930.

[31] Guo, F., Chen, Z., Huang, X., Cao, L., Cheng, X., Shi, W., Chen, L. (2021). Cu_3P nanoparticles decorated hollow tubular carbon nitride as a superior photocatalyst for photodegradation of tetracycline under visible light. *Separation and Purification Technology*, 275, 119223. DOI: 10.1016/j.seppur.2021.119223.

[32] Zhao, S., Chen, J., Liu, Y., Jiang, Y., Jiang, C., Yin, Z., Xiao, Y., Cao, S. (2019). Silver nanoparticles confined in shell-in-shell hollow TiO_2 manifesting efficiently photocatalytic activity and stability. *Chemical Engineering Journal*, 367, 249–259. DOI: 10.1016/j.cej.2019.02.123.

[33] Qamar, M.A., Shahid, S., Javed, M., Iqbal, S., Sher, M., Bahadur, A., AL-Anazy, M.M., Laref, A., Li, D. (2021). Designing of highly active g-C_3N_4/Ni-ZnO photocatalyst nanocomposite for the disinfection and degradation of the organic dye under sunlight radiations. *Colloids and Surfaces A: Physicochemical and Engineering Aspects*, 614, 126176. DOI: 10.1016/j.colsurfa.2021.126176.

[34] Qamar, M.A., Javed, M., Shahid, S., Sher, M. (2022). Fabrication of g-C3N4/transition metal (Fe, Co, Ni, Mn and Cr)-doped ZnO ternary composites: Excellent visible light active photocatalysts for the degradation of organic pollutants from wastewater. *Materials Research Bulletin*, 147, 111630. DOI: 10.1016/j.materresbull.2021.111630.

[35] Ahmad, I. (2020). Comparative study of metal (Al, Mg, Ni, Cu and Ag) doped ZnO/g-C_3N_4 composites: Efficient photocatalysts for the degradation of organic pollutants. *Separation and Purification Technology*, 251, 117372. DOI: 10.1016/j.seppur.2020.117372.

[36] Raha, S., Ahmaruzzaman, M. (2020). Enhanced performance of a novel superparamagnetic g-C3N4/NiO/ZnO/Fe_3O_4 nanohybrid photocatalyst for removal of esomeprazole: Effects of reaction parameters, co-existing substances and water matrices. *Chemical Engineering Journal*, 395, 124969. DOI: 10.1016/j.cej.2020.124969.

[37] Bajiri, M.A., Hezam, A., Namratha, K., Viswanath, R., Drmosh, Q.A., Naik, H.S.B., Byrappa, K. (2019). CuO/ZnO/g-C_3N_4 heterostructures as efficient visible light-driven photocatalysts. *Journal of Environmental Chemical Engineering*, 7(5), 103412. DOI: 10.1016/j.jece.2019.103412.

[38] Lee, S.J., Begildayeva, T., Jung, H.J., Koutavarapu, R., Yu, Y., Choi, M., Choi, M.Y. (2021). Plasmonic ZnO/Au/g-C_3N_4 nanocomposites as solar light active photocatalysts for degradation of organic contaminants in wastewater. *Chemosphere*, 263, 128262. DOI: 10.1016/j.chemosphere.2020.128262.

[39] Sheydaei, M., Ayoubi-Feiz, B., Abbaszade-Fakhri, G. (2021). A visible-light active g-C_3N_4/Ce–ZnO/Ti nanocomposite for efficient photoelectrocatalytic pharmaceutical degradation: Modelling with artificial neural network. *Process Safety and Environmental Protection*, 149, 776–785. DOI: 10.1016/j.psep.2021.03.037.

[40] Thi, T.A.N., Vu, A.T. (2022). Nanocomposite ZnO/g-C_3N_4 for Improved Degradation of Dyes under Visible Light: Facile Preparation, Characterization, and Performance Investigations. *Bulletin of Chemical Reaction Engineering & Catalysis*, 17(2), 403–419. DOI: 10.9767/bcrec.17.2.13931.403-419.